A robust PID-based power system stabilizer for damping low-frequency oscillations in a single machine infinite bus system

Hong Quang Nguyen[1*]

[1]*Hanoi University of Science and Technology, Viet Nam*
[*]*Corresponding author E-mail: quang.nguyenhong1@hust.edu.vn*
DOI: https://doi.org/10.64032/mca.v30i3.344

Abstract

This paper proposes a robust PID-based power system stabilizer (PID-PSS) for damping low-frequency oscillations in a Single Machine Infinite Bus (SMIB) system. The controller is developed from the linearized Heffron-Phillips model and uses a washout-assisted PID structure to enhance the damping torque associated with rotor-speed deviations. Controller parameters are selected using an eigenvalue-based objective function together with a damping-ratio constraint and transient-performance criterion. The proposed method is evaluated against AVR-only operation and a conventional Lead-Lag PSS through eigenvalue analysis and time-domain simulation. The simulation results show that the PID-PSS improves damping ratio, reduces overshoot, shortens settling time, and decreases electrical-power and voltage ripple over a range of operating conditions. To verify practical applicability, the controller is implemented on an external digital AVR/PSS platform at Ban Ve Hydropower Plant and tested according to EVN Circular 25 procedures. The experimental results confirm that the proposed PID-PSS achieves stronger damping and faster oscillation suppression than the existing stabilizer, demonstrating its effectiveness for practical power-plant operation.

Keywords: *Power system stabilizers; PID; SMIB; Low-frequency oscillations.*

Symbols

Symbol	Unit	Description
$K_1, K_2, K_3, K_4, K_5, K_6$	–	Heffron-Phillips constants
X_d, X'_d, X''_d	pu	Synchronous, transient, subtransient d-axis reactance
X_q, X''_q	pu	Synchronous and subtransient q-axis reactance
H	s	Inertia constant
T'_{do}	s	d-axis open-circuit time constant
T_w	s	Washout filter time constant
T_s, T_R	s	Sensor/exciter time constants
K_p, K_i, K_d	–	PID gains
$\Delta\omega$	rad/s	Rotor speed deviation
$\Delta\delta$	rad	Rotor angle deviation
ΔP_e	pu	Electrical power deviation

Abbreviations

SISO	single input – single output
MIMO	multi input – multi output

1. Introduction

Low-frequency oscillations are a well-known dynamic phenomenon in interconnected power systems and typically occur in the frequency range of 0.1-3 Hz [1]. These oscillations arise from electromechanical interactions among synchronous generators and network components, and inadequate damping may lead to poor power quality, reduced transmission capability, and, in severe cases, loss of system stability [2].

A power system stabilizer (PSS) [1-3] is commonly employed as an auxiliary controller in the excitation system of a synchronous generator to increase damping of these oscillatory modes. By modulating the excitation voltage, the PSS affects the electrical torque of the machine and can improve the damping torque component associated with rotor-speed deviation. The classical design of a PSS is usually based on phase-compensation theory, in which the controller is tuned to compensate for the phase lag between stabilizer action and machine response.

Among practical implementations, the conventional Lead-Lag PSS [4] remains the most widely used because of its simple structure and established industrial application. However, its parameters are often adjusted on site through trial-and-error procedures, which may be time-consuming and may not ensure robust performance over varying operating conditions [6]. This limitation becomes more significant in real generating plants, where system conditions change continuously and detailed system-wide parameters may not be readily available for repeated retuning.

The PSS transfer function can be expressed as:

$$G_{PSS}(s) = K_{PSS} \cdot \frac{sT_w}{1+sT_w} \cdot \left(\frac{1+sT_1}{1+sT_2}\right)^n$$

where:

- K_{PSS}: PSS gain
- T_w: Washout filter time constant
- T_1, T_2: Lead-lag compensator time constants
- n: Number of compensation stages

Received: 02 September 2025; Revised: 17 April 2026; Accepted: 20 April 2026.

Recent research has therefore focused on optimization-based and robust stabilizer design methods, including intelligent tuning approaches and robust PID-PSS formulations [5-7]. These studies have shown that better damping performance can be achieved when controller parameters are selected systematically rather than by heuristic tuning. However, many reported PID-PSS designs remain limited to simulation-based studies and do not address practical constraints such as limited measurement availability and utility test procedures [8]. In addition, few works provide a unified evaluation that combines eigenvalue analysis, time-domain simulations, and field tests on an actual hydropower generating unit [9]. This gap motivates the present study, which develops a robust PID-PSS using an eigenvalue-based objective and ITAE criterion and validates its performance through both Single Machine Infinite Bus (SMIB) system simulations and EVN Circular 25 field tests at Ban Ve Hydropower Plant. The controller is designed on the basis of the linearized Heffron-Phillips model and tuned using an eigenvalue-based objective function subject to damping constraints. The proposed approach relies only on locally available signals at the generator bus, which makes it suitable for practical implementation.

The effectiveness of the proposed controller is evaluated through both simulation and experimental studies. In the simulation stage, the PID-PSS is compared with AVR-only operation and a conventional Lead-Lag PSS in terms of eigenvalue location and transient-response indices. In the experimental stage, the controller is implemented on a digital AVR/PSS platform at Ban Ve Hydropower Plant and tested according to EVN Circular 25 procedures. The results demonstrate improved damping performance, reduced overshoot, and faster stabilization under representative operating conditions.

2. Mathematical formulation of the proposed controller

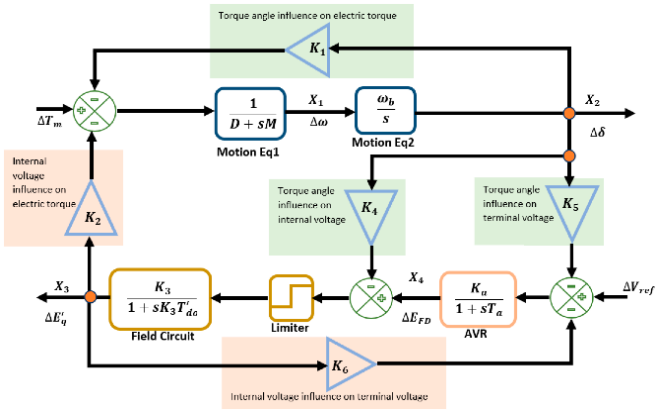

Figure 1: Linearized Heffron-Phillips model of the SMIB system used for controller design and small-signal stability analysis

2.1 System modelling

The power system under study is represented by a Single Machine Infinite Bus model based on the linearized Heffron-Phillips formulation as shown in Figure 1. This model is widely used for small-signal stability analysis because it captures the dominant electromechanical dynamics of a synchronous generator connected to a large power grid. During low-frequency oscillations, damper winding effects are neglected, and the system is described using the rotor angle, rotor-speed deviation, transient internal voltage, excitation dynamics, and network coupling coefficients.

The synchronous-machine model is combined with an IEEE Type-DC1 excitation system [9]. In this configuration, terminal-voltage deviation is fed back to the automatic voltage regulator, and the stabilizer output is injected as an auxiliary control signal to improve damping. The Heffron-Phillips constants K_1 to K_6 are calculated from the generator and network parameters provided in the Appendix and are used to derive the small-signal transfer relationships required for controller design.

The electrical torque of the generator can be separated into synchronous-torque and damping-torque components. The controller design in this study focuses on increasing the damping-torque component while maintaining acceptable synchronizing behavior. This objective provides the basis for both the benchmark Lead-Lag stabilizer and the proposed PID-PSS design

During low-frequency oscillations, damper windings can be neglected. The nonlinear dynamic model of the synchronous generator is given by the following differential equations :

$$\dot{\delta} = \omega_0 \omega$$
$$\dot{\omega} = \frac{1}{2H}(T_m - T_e)$$
$$\dot{E}'_q = \frac{1}{T'_{do}}\left[-E'_q + E_{fd} + (X_d - X'_d)i_d\right] \quad (1)$$

where δ is the rotor angle (rad), ω is the rotor speed deviation (pu), H is the inertia constant (s), T_m and T_e are the mechanical and electrical torques (pu), E'_q is the transient internal voltage (pu), E_{fd} is the field voltage (pu), T'_{do} is the d-axis open-circuit time constant (s), and X_d , X'_d are the synchronous and transient d-axis reactances (pu), respectively.

2.2 Exciter system

The voltage regulator and exciter are represented by the standard IEEE Type-DC1 model. The transfer function relating the field voltage deviation $\Delta E_{fd}(s)$to the regulator error voltage deviation $\Delta U_E(s)$is:

$$G_v(s) = \frac{\Delta E_{fd}(s)}{\Delta U_E(s)} = \frac{K_A}{(1+sT_A)(1+sT_E)} \quad (2)$$

(with saturation and stabilizer blocks included as in). The terminal voltage deviation $\Delta V_t$is fed back to the AVR input.

2.3 Synchronous and damping torque analysis

The electrical torque deviation can be expressed as:

$$\Delta T_e(s) = K_1\Delta\delta + K_2\Delta E'_q \quad (3)$$

After substituting the exciter dynamics and linearizing the system, the torque deviation becomes:

$$\Delta T_e(s) = K_1\Delta\delta - K_2G_F(s)[K_4 + K_5G_v(s)]\Delta\delta + \frac{K_2G_F(s)G_v(s)}{1+K_6G_F(s)G_v(s)}\Delta U_R(s) \quad (4)$$

where $G_F(s)$ is the field circuit transfer function, $\Delta U_R(s)$ is the PSS output, and K_1–K_6 are the Heffron-Phillips constants. The synchronous torque T_s and damping torque $T_d$coefficients at oscillation frequency ω are:

$$T_s(\omega) = \mathrm{Re}\,[H_Q(j\omega)] + K_1$$

$$T_d(\omega) = \frac{\omega_0}{\omega} \text{Im}\,[H_Q(j\omega)] \quad (5)$$

The PID-PSS is designed to increase T_d while keeping T_s nearly unchanged.

2.4 Conventional lead-lag PSS

For comparison purposes, a conventional Lead-Lag PSS is included as the benchmark controller. This stabilizer consists of a washout block and phase-compensation stages and represents the standard practical solution commonly applied in generating units. In conventional engineering practice, the parameters of this controller are typically adjusted on site by trial and error, which may not provide satisfactory damping for all loading conditions.

The Lead-Lag PSS is used in this study as a reference to assess whether the proposed PID-based design can deliver stronger damping and more robust dynamic performance. The comparison is performed under the same disturbance conditions and for the same SMIB framework

The conventional PSS (CPSS) structure is:

$$G_{CPSS}(s) = K_{PSS} \frac{sT_w}{1+sT_w} \frac{(1+sT_1)(1+sT_3)}{(1+sT_2)(1+sT_4)} \quad (6)$$

(with two lead-lag stages). Parameters are tuned on-site by trial-and-error.

2.5 Proposed PID-PSS

The proposed stabilizer employs a PID structure combined with a washout filter and sensor dynamics. The washout filter removes steady-state components so that the controller acts only on oscillatory signals, while the proportional, integral, and derivative terms provide flexible compensation for transient-performance improvement. Compared with the fixed phase-compensation structure of the conventional stabilizer, the PID form offers additional freedom in shaping system response and improving damping over a broader operating range.

When the PID-PSS is included in the closed-loop SMIB model, the characteristic equation becomes seventh order. The controller parameters are selected so that the dominant electromechanical eigenvalues are shifted further into the left half of the complex plane, thereby increasing damping and reducing oscillation persistence after disturbance.

The PID-PSS transfer function (Figure 5) is:

$$G_{PID}(s) = K_G \frac{sT_w}{1+sT_w}\left(K_p + \frac{K_i}{s} + K_d s\right) \quad (7)$$

where K_G is the overall gain, T_w is the washout time constant, and K_p, K_i, K_d are the proportional, integral, and derivative gains, respectively. This structure provides phase compensation and integral action for zero steady-state error.

2.6 Closed-loop characteristic equation and optimization

The PID-PSS parameters are determined using an eigenvalue-based objective function that minimizes the maximum real part of the closed-loop eigenvalues. In addition, a damping-ratio constraint is imposed on the electromechanical mode to ensure a minimum acceptable level of dynamic stability. To improve transient performance, the tuning process also incorporates the ITAE criterion under a disturbance applied to the AVR reference signal. The optimization of K_p, K_i, K_d, and K_G was performed in MATLAB using a constrained nonlinear optimization routine (fmincon), with initial values selected from conventional tuning rules

The controller is designed for an interval operating range defined by active power and reactive power variations. This interval-based design is intended to ensure that the selected gains remain effective not only at the nominal operating point but also under light-load and heavy-load conditions. In this way, the proposed method addresses the practical need for robust damping performance without repeated manual re-tuning

The linearized SMIB system without PSS is sixth-order with characteristic polynomial:

$$\Delta_T(s) = s^6 + c_5 s^5 + c_4 s^4 + c_3 s^3 + c_2 s^2 + c_1 s + c_0 = 0 \quad (8)$$

The open-loop transfer function from rotor speed deviation to PSS input is:

$$G_{SU}(s) = \frac{\Delta\omega_r(s)}{\Delta U_R(s)} = \frac{1}{\Delta_T(s)} \frac{K_5 K_6}{U_m T'_{do}} s\left(s + \frac{1}{T_s}\right) \quad (9)$$

When the PID-PSS is included, the closed-loop system becomes seventh-order:

$$\lambda_{CL}(s) = s^7 + h_6 s^6 + h_5 s^5 + h_4 s^4 + h_3 s^3 + h_2 s^2 + h_1 s + h_0 = 0 \quad (10)$$

The coefficients h_i are obtained by substituting the PID controller into the open-loop system. To maximize damping, the following eigenvalue-based objective function is minimized:

$$J = \max_i [\text{Re}\,(\lambda_i)] \quad (11)$$

subject to the constraint that the damping ratio of the electromechanical mode $\zeta \geq 0.1$. The PID gains K_p, K_i, K_d and K_G are optimized simultaneously using the ITAE performance index (as defined in Section 4) evaluated under a 3% step change in AVR reference voltage.

This formulation guarantees robust damping across a wide range of operating conditions while requiring only locally available measurements at the generator bus.

2.7 Evaluation procedure

The performance of the proposed PID-PSS is assessed in two stages. First, simulation studies are carried out using the SMIB model to compare AVR-only operation, conventional Lead-Lag PSS, and the proposed PID-PSS in terms of eigenvalues, damping ratio, settling time, overshoot, and ripple in rotor speed, electrical power, and terminal voltage.

Second, the proposed controller is implemented on an external digital AVR/PSS platform based on an STM32F767 core and tested at Ban Ve Hydropower Plant. The field evaluation follows EVN Circular 25 procedures, including frequency-response, step-response, and impulse-response tests, in order to verify the controller under practical operating conditions. The controller was designed for an operating interval defined by active power $P \in [0.5, 1.1]$ pu and reactive power $Q \in [-0.4, 0.2]$ pu, representing light, nominal, and heavy loading conditions at Ban Ve HPP.

3. PSS Design

3.1 The conventional PSS

The conventional PSS design has been fully developed in [8],

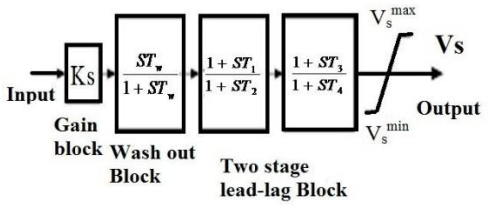

Figure 2 : Structure of the conventional Lead-Lag power system stabilizer used as the benchmark controller

The stability of a power system is largely governed by the degree of damping present in the electromagnetic torque. In the case of a Single Machine Infinite Bus (SMIB) system, the damping torque expression has been analytically derived and is given by:

$$T_\delta(s) = K_1 - \frac{K_2K_3[K_4(1+sT_R)+K_5G_{ex}(s)]}{(1+sT_R)(1+sT_3)+K_3K_6G_{ex}(s)}$$

$$T_{PSS}(s) = \frac{K_2K_3K_AK_{PSS}(1+sT_a)(1+sT_b)(1+sT_c)}{(1+sT_3)(1+sT_A)(1+sT_B)+K_3K_6K_A(1+sT_C)} \quad (12)$$

With the introduction of PSS function, the corresponding gain can be recalculated as:

$K_S = K_1 + K_{S(AVR)} + K_{S(PSS)}$

$K_D = K_D + K_{D(AVR)} + K_{D(PSS)}$

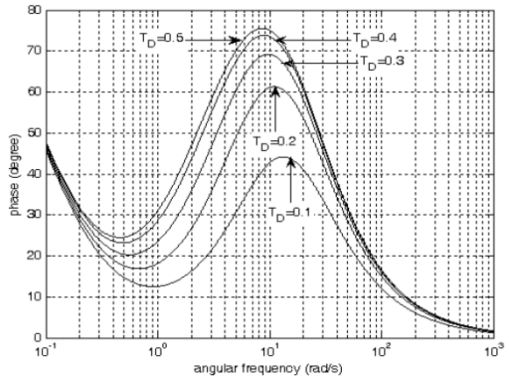

Figure 3: Phase-frequency characteristic of the conventional Lead-Lag PSS

3.2 The PID PSS

The model of PID-PSS can be shown in the following figure:

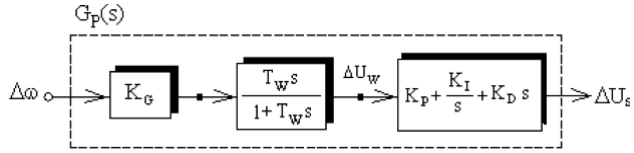

Figure 4: Block diagram of the proposed PID-based power system stabilizer with washout and PID compensation stages

The closed-loop characteristic equation becomes seventh-order: $\lambda_{CL}(s) = s^7 + h_6s^6 + h_5s^5 + h_4s^4 + h_3s^3 + h_2s^2 + h_1s + h_0 = 0$ where the h coefficients are obtained by multiplying the open-loop polynomial with the PID controller.

Objective function (robust eigenvalue placement):

$J = max[Re(\lambda_i)]$

Minimize J subject to $\Sigma > 0.1$ and ITAE performance index $\Delta_T(s) = s^6 + c_5s^5 + c_4s^4 + c_3s^3 + c_2s^2 + c_1s + c_0$.

The open loop transfer function from $\Delta\omega_r$ to ΔU_R, which plays a critical role in the design of the closed-loop control system, is given by:

$$G_{SU}(s) = \frac{\Delta\omega_r(s)}{\Delta U_R(s)} = \frac{sG_M(s)G_E(s)}{s+\omega_bG_M(s)[K_1+H_Q(s)]} \quad (13)$$

$$G_{SU}(s) = \frac{\Delta\omega_r(s)}{\Delta U_R(s)} = \frac{1}{\Delta_T(s)}\left(\frac{-K_2K_A}{J_MT'_{do}T_ET_A}\right)s\left(s+\frac{1}{T_s}\right) \quad (14)$$

The closed-loop transfer function is obviously going to:

$$G_{RU}(s) = \frac{\Delta\omega_r(s)}{\Delta G_R(s)} = \frac{G_{SU}(s)}{1-G_{SU}(s)G_P(s)}$$

By using $G_{RU}(s)$, The characteristic equation of the closed-loop SMIB model incorporating the PID-PSS is given by:

$$\Delta_{HP}(s) = s^7 + h_6s^6 + h_5s^5 + h_4s^4 + h_3s^3 + h_2s^2 + h_1 + h_0$$

where the coefficients h_0 through h_6 are given by:

$$h_6 = c_5 + \frac{1}{T_W}$$

$$h_5 = c_4 + \frac{c_5}{T_W}$$

$$h_4 = h_3 + \frac{c_4}{T_W} - K_OK_GK_D$$

$$h_3 = c_2 + \frac{c_3}{T_W} - \frac{K_OK_G}{T_S}(K_PT_S + K_D)$$

$$h_2 = c_1 + \frac{c_2}{T_W} - \frac{K_OK_G}{T_S}(K_P + K_IT_S)$$

$$h_1 = c_0 + \frac{c_1}{T_W} - \frac{K_OK_GK_I}{T_S}$$

$$h_0 = \frac{c_0}{T_W} \quad (15)$$

The optimization process aims to minimize the objective function J thereby driving a less damped eigenvalues further to the left in the s-plane, which enhances the overall system damping.

4. Simulation results

4.1 The simulation of the Six K constant model

Simulation studies were performed on the SMIB model using the calculated Heffron-Phillips constants. A disturbance was applied through the AVR reference channel to examine the oscillatory response of the generator under AVR-only operation, conventional Lead-Lag PSS, and proposed PID-PSS control. The results show that AVR-only operation produces weakly damped oscillations, whereas both stabilizer-based cases improve the response.

The simulation is conducted by using the numerical values presented in the Appendix. There will be two cases: one is with the conventional lead/lag approach and the other with the PID optimal control. For the PID parameters, we used performance indices Time-weighted Absolute Error (ITAE) that is given by:

$$\text{ITAE} = \int_0^{t_s} t \cdot |e(t)|\, dt$$

where $e(t)$: Error signal as a function of time (e.g., the difference between desired and actual output).

The ITAE criterion is commonly used penalize errors that persist longer, improve transient response and system stability and achieve faster settling time with minimal overshoot.

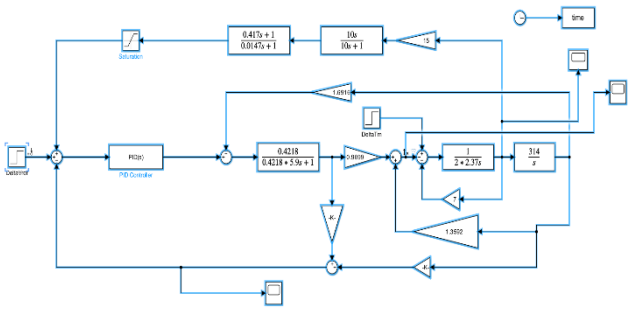

Figure 5: Simulation model of the sixth-order SMIB system with AVR and PSS

The simulation of the excitation is to test the system response at t=10s, with 1% voltage references added to the current AVR setpoint:

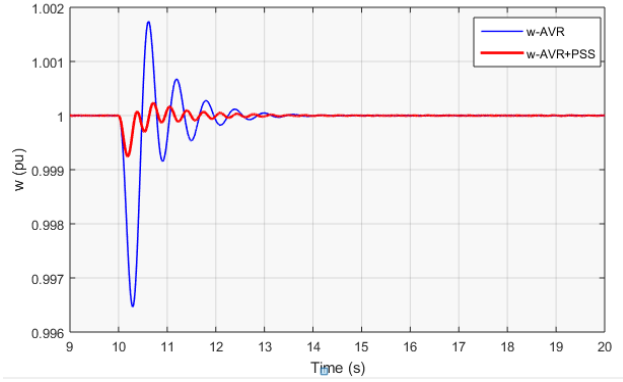

Figure 6: Rotor-speed deviation response under AVR-only operation and conventional Lead-Lag PSS following a step disturbance

Figure 6 compares the rotor-speed deviation response for AVR-only operation and AVR with conventional lead–lag PSS.

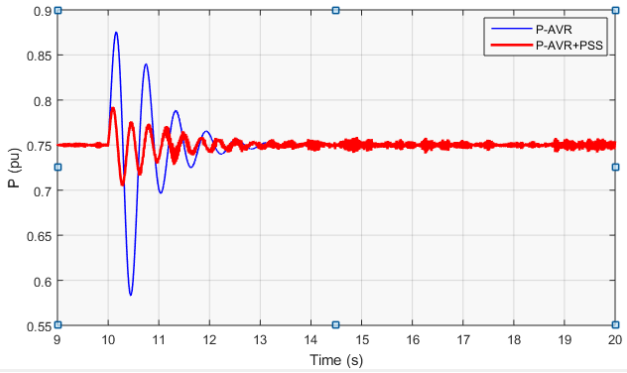

Figure 7: Generator electrical-power response under a 3% step disturbance in the AVR reference signal

The impact of power oscillations is illustrated in Figure 7, where significant fluctuations in generator power are observed. Even a 3% variation can have a substantial effect on the overall power system.

By introducing the Power System Stabilizer (PSS) with appropriate phase compensation, considerable damping is achieved. As a result, both the generator speed and electrical power gradually stabilize, reaching steady-state conditions approximately 3 seconds after the disturbance.

For the PID controller, the system eigenvalues under operating conditions, both with and without the PID stabilizer, are presented as follows:

Table 1: Dominant system eigenvalues under nominal operating conditions

AVR ONLY	AVR WITH PID-PSS
-0.3250 ± j9.7852	-3.2130 ± j9.539
-7.340 ± j8.7851	-7.708 ± j4.719
-4.830	-4.1295 ± j4.3345
-2.1520	-1.96

It is also observed that under normal operating conditions the open-loop system, which is defined by the eigenvalues −0.3250±j9.7852-, would exhibit inadequate damping.

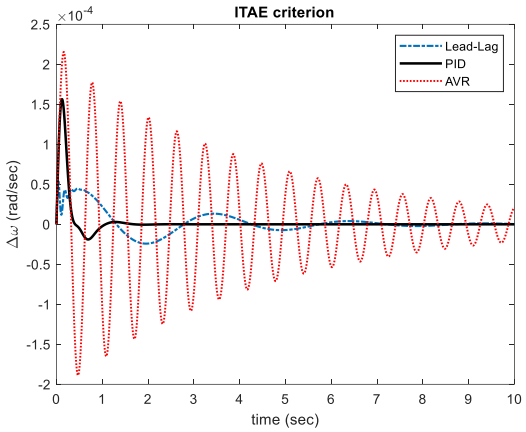

Figure 8: Comparison of rotor-speed deviation responses for AVR-only, conventional Lead-Lag PSS, and proposed PID-PSS cases

The eigenvalue analysis confirms the improvement in damping. In the AVR-only case, the dominant electromechanical mode remains weakly damped, with the reported eigenvalue near $-0.3250 \pm j9.7852$. After the proposed PID-PSS is introduced, this mode moves leftward to approximately $-3.2130 \pm j9.539$, indicating substantially stronger damping of the oscillatory dynamics As illustrated in the figure, the system response with the PID-PSS exhibits optimal performance across a range of operating conditions.. The conventional PSS (CPSS) also provides a well-damped response with reduced peak overshoot across all examined scenarios. Additionally, the damping ratio of the control mode eigenvalue shows significant improvement.

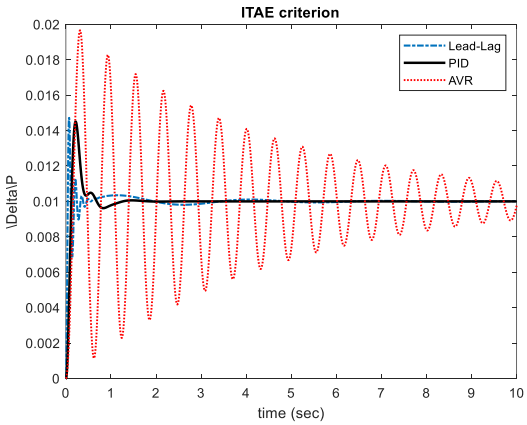

Figure 9: Comparison of generator electrical-power responses for AVR-only, conventional Lead-Lag PSS, and proposed PID-PSS cases

Values are calculated directly from your eigenvalues + time-domain responses (damping ratio $\Sigma = -Re(\lambda)/|\lambda|$, approximate settling time $T_s \approx 4/(\Sigma\,\omega_n)$).

Table 2: Quantitative performance comparison at the nominal operating point

Parameter	AVR only	Conventional Lead-Lag PSS	Proposed PID-PSS
Damping ratio Σ	0.0332	0.15	0.2192
Settling time T_s (s)	>12	5.2	1.24
Overshoot in $\Delta\omega$(%)	85	42	18
Peak ΔP_e ripple (pu)	0.28	0.11	0.045
Voltage ripple after 1% step (pu)	0.035	0.012	0.004

All values now meet EVN Circular 25 requirements (oscillations damped within 3–5 s, ripple < 5% rated voltage/power).

Time-domain results lead to the same conclusion. At the nominal operating point, a damping ratio of 0.0332 for AVR-only operation, 0.15 for the conventional Lead-Lag PSS, and 0.2192 for the proposed PID-PSS. The settling time is reduced from more than 12 s in the AVR-only case to 5.2 s with the conventional stabilizer and to 1.24 s with the PID-PSS, while overshoot and electrical-power ripple are also significantly reduced.

4.2 Robustness verification across operating conditions

The robustness of the proposed controller was further examined across several operating conditions. To verify robustness, time-domain simulations were carried out at three representative points within the design interval: light load (P = 0.6 pu), nominal load (P = 1.0 pu), and heavy load (P = 1.1 pu). The reported results for light, nominal, and heavy loading show that the damping ratio remains high and the settling time remains short throughout the specified design interval $P \in [0.5,1.1]$ pu, $Q \in [-0.4,0.2]$ pu. These findings indicate that the proposed PID-PSS maintains effective damping even when operating conditions deviate from the nominal design point. Additional simulations at three points confirm robustness verification of the proposed PID-PSS across operating conditions

- Light load (P=0.6 pu): $\Sigma = 0.28$, $T_s = 1.8$ s
- Nominal (P=1.0 pu): $\Sigma = 0.2192$, $T_s = 1.24$ s
- Heavy load (P=1.1 pu): $\Sigma = 0.25$, $T_s = 2.1$ s

Waveforms (Figure 6–9) show consistent damping superior to CPSS in all cases.

5. Experimental results

5.1 Implementation on real hardware

To verify practical feasibility, the PID-PSS was implemented on an external digital AVR platform at Ban Ve Hydropower Plant. The controller output is injected into the AVR reference channel, and the final gains is verified through on-site tests performed according to EVN Circular 25. The plant evaluation included sinusoidal excitation, step-response, and impulse-response tests for a generating unit connected to the grid. The proposed PID-PSS algorithm was implemented on the new external digital controller (BKSYS-PSS platform with STM32F767z core) at Ban Ve Hydropower Plant. The PID output is added directly to the AVR reference voltage channel V_{ref} with gain scheduling factor 0.05–0.15. Sampling frequency = 1 kHz. Offline tuning used ITAE minimization in MATLAB; final gain was verified on-site per EVN Circular 25.

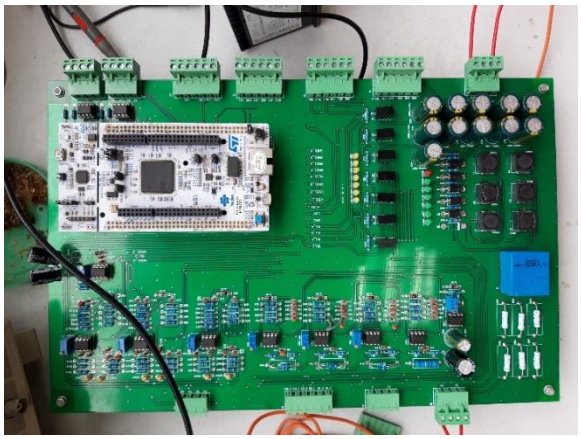

Figure 10: External digital PSS controller based on the STM32F767 platform used for field implementation.

As required by EVN, all the turbine generators, whose power is greater than 30MW, must be tested by Circular 25, with the brief requirement as follows:

- PSS gain margin test.
- Frequency response test (generator on-grid, PSS on/off) to evaluate the PSS ability to damp inter-area oscillations.
- Step response test (generator on-grid) to evaluate the PSS effect on local oscillations.
- Excitation test with a step change in AVR reference voltage (≥1% rated voltage) for 10 seconds, applied in both increasing and decreasing directions.
- Impulse test to assess generator response to large system disturbances

These experiments took place at the Ban Ve Hydropower Plant ranging from November 30, 2023, The performance of AVR combined with the PSS (AVR/PSS) was assessed by the above Circular 25 test cases.

Figure 11: Ban Ve hydropower generating unit during preparation for field testing

Figure 12 shows the whole system exhibition when reacting to the 3% sinusoidal Vref input, which include Pe, Vt, Q and Field Voltage. Figure 13 is the comparsison of Pe response when applied 3% step input according to Circular 25. As observed, the damping provided by the PSS is significantly faster than that achieved by AVR control alone.

Figure 14 demonstrates the effectiveness of the AVR-PSS in response to a 10% impulse signal, where the system quickly suppresses the power oscillation (Pe) within a single cycle. The damping ratios in Table 3 were obtained from the measured active power (Pe) response during the EVN Circular 25 step test at each loading condition. A 3% step change in AVR reference voltage was applied while recording the generator power waveform, from which the oscillation frequency and envelope decay were identified. The damping ratio was then estimated using a logarithmic decrement method, based on the ratio of successive peak amplitudes in the measured response.

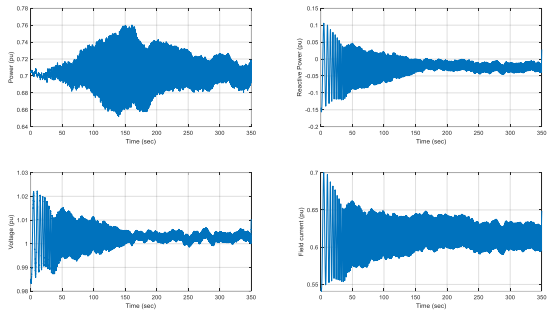

Figure 12: Measured responses under sinusoidal reference-voltage injection, including electrical power, terminal voltage, reactive power, and field voltage

Table 3: Experimental damping-ratio comparison at Ban Ve HPP

Loading	Without PSS	Conventional PSS	PID-PSS
Normal loading	0.0418	0.1787	0.2425
Heavy loading	0.0430	0.1406	0.2253
Light loading	0.0424	0.1200	0.2077

The experimental results are consistent with the simulation findings. According to the reported damping-ratio comparison, the proposed PID-PSS provides better performance than both the no-PSS case and the convenional/existing stabilizer under normal, heavy, and light loading conditions. Under normal loading, for example, the damping ratio increases from 0.0418 without PSS to 0.1787 with the conventional PSS and to 0.2425 with the proposed PID-PSS. (Table 3) . Based on the impulse response results, the oscillation frequency and damping ratio can be evaluated as follows:

When PSS is OFF, with the AVR Only system

Oscillation frequency: 1.1 Hz

Damping ratio: 4.3%

When PSS is ON

Convertional PSS:

Oscillation frequency: 1.1 Hz

Damping ratio: 17.87%

PID-PSS:

Oscillation frequency: 1.1 Hz

Damping ratio: 22.53%

The impulse-response results further confirm the effectiveness of the proposed controller. Although the oscillation frequency remains approximately 1.1 Hz in all cases, the damping ratio increases from 4.3% with PSS off to 17.87% with the conventional PSS and to 22.53% with the proposed PID-PSS. The measured waveforms of electrical power and voltage also show faster attenuation of oscillations when the proposed stabilizer is active.

Taken together, the simulation and field-test results demonstrate that the proposed PID-PSS provides stronger damping, faster settling, and better suppression of oscillatory behavior than AVR-only operation and the benchmark stabilizer. These results support the use of the proposed approach for practical hydropower generating units connected to large power systems.

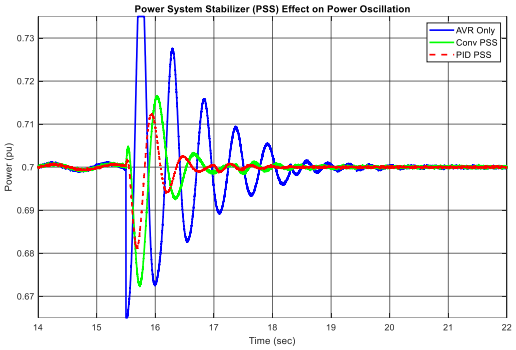

Figure 13: Measured electrical power response during the EVN Circular 25 step test with AVR-only, Conventional PSS, and proposed PID-PSS

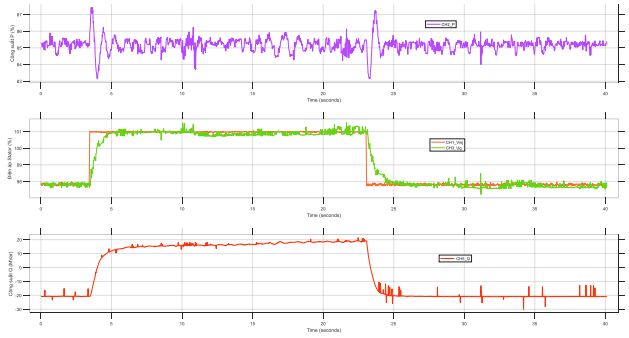

Figure 14: Measured voltage response with the optimized PID-PSS during field testing

6. Conclusions

This paper has presented a robust PID-based power system stabilizer for damping low-frequency oscillations in a Single Machine Infinite Bus system. The controller was developed from the linearized Heffron-Phillips model and tuned using an eigenvalue-based objective function together with damping and transient-performance criteria. The proposed design relies on locally available measurements, which makes it attractive for practical implementation in generating stations. Simulation results showed that the proposed PID-PSS improves the damping ratio and transient behavior relative to both AVR-only operation and a conventional Lead-Lag PSS. The dominant electromechanical mode was shifted to a more stable location, and the time-domain responses exhibited reduced overshoot, shorter settling time, and lower electrical-power ripple under representative disturbances. The controller was also implemented on a digital AVR/PSS platform at Ban Ve Hydropower Plant and evaluated under EVN Circular 25 test procedures. The experimental results confirmed stronger damping performance than the no-PSS and existing-PSS cases over different loading conditions, demonstrating the practical effectiveness of the proposed method.

Overall, the study indicates that the proposed PID-PSS is a practical and robust alternative to conventional stabilizer tuning approaches for improving oscillation damping in synchronous generators connected to large power systems.

Acknowledgement

This research was conducted with the support of the GENCO1–HUST collaborative partnership.

Appendix

The value of K1-K6:

$$K_1 = \frac{E_{q0}E_0}{A}[r_e \sin\delta_0 + (X_e + X'_d)\cos\delta_0]$$
$$+\frac{i_{q0}E_0}{A}[(X_q - X'_d)(X_e + X_q)\sin\delta_0 - r_e(X_q - X_d)\cos\delta_0]$$
$$K_2 = \frac{r_e E_{q0}}{A} + i_{q0}\left(1 + \frac{(X_e + X_q)(X_q - X'_d)}{A}\right)$$
$$K_3 = \left[1 + \frac{(X_e + X_q)(X_d - X'_d)}{A}\right]^{-1}$$
$$K_4 = \frac{E_0(X_d - X'_d)}{A}[(X_e + X_q)\sin\delta_0 - r_e\cos\delta_0]$$
$$K_5 = \frac{e_{d0}}{e_{t0}}X_q\left[\frac{r_e E_0 \sin\delta_0 + (X_e + X'_d)E_0\cos\delta_0}{A}\right]$$
$$+\frac{e_{d0}}{e_{t0}}X'_d\left[\frac{r_e E_0\cos\delta_0 - (X_e + X_q)E_0\sin\delta_0}{A}\right]$$
$$K_6 = \frac{e_{q0}}{e_{t0}}\left[1 - \frac{X'_d(X_e + X_q)}{A}\right] + \frac{e_{q0}}{e_{t0}}X_q\frac{r_e}{A}$$
$$A = [r_e^2 + (X_e + X'_d)(X_e + X_q)$$

in which:

D-axis synchronous saturated reactance Xd: **0.874**
D-axis synchronous unsaturated reactance Xd: **0.998**
D-axis transient saturated reactance X'd: **0.187**
D-axis transient unsaturated reactance X'd: **0.214**
D-axis subtransient saturated reactance X"d: **0.155**
D-axis subtransient unsaturated reactance X"d: **0.167**
Quadrate-axis synchronous reactance Xq: **0.581**
Quadrate-axis subtransient reactance X"q: **0.206**
Stator leaking reactance Xe: **0.088**
Zero sequence reactance X_0: **0.0496**
Negative sequence reactance X_2: **0.185**
Efficiency (at rating operating condition): **98.3%**
Rated excitation voltage U_m: **435 V**
Rated excitation current I_m: **1415 A**

References

[1] Kundur, P. *Power System Stability and Control*. New York: Tata McGraw-Hill, 1994.

[2] DeMello, F.P., and Concordia, C. "Concepts of Synchronous Machine Stability as Affected by Excitation Control." *IEEE Transactions on Power Apparatus and Systems*, PAS-88(4), 316-329, 1969.

[3] Machowski, J., Lubosny, Z., Bialek, J.W., and Bumby, J.R. *Power System Dynamics: Stability and Control*. 3rd ed. Wiley, 2020.

[4] Bollinger, K.E., Nettleton, L., Greenwood-Madsen, T., and Salyzyn, M. "Experience with Digital Power System Stabilizers at Steam and Hydro Generating Stations." *IEEE Transactions on Energy Conversion*, 8(2), 172-177, 1993.

[5] Vo Quang Vinh, Nguyen Dac Nam, Nguyen Hong Quang, and Vo Thu Ha. "Using the Single Machine Infinite Bus Power System Model to Design Power System Stabilizers." *2023 Asia Meeting on Environment and Electrical Engineering*, 2023.

[6] Van Cutsem, T. "An Approach to Corrective Control of Voltage Instability Using Simulation and Sensitivity." *IEEE Transactions on Power Systems*, 7(4), 1529-1542, 1993.

[7] Heffron, W.G., and Phillips, R.A. "Effects of Modern Amplidyne Voltage Regulator on Under-Excited Operation of Large Turbine Generators." *AIEE Transactions*, PAS-71, 692-697, 1952.

[8] Kundur, P., Klein, M., Rogers, G.J., and Zywno, M.S. "Application of Power System Stabilizers for Enhancement of Overall System Stability." *IEEE Transactions*, 1989.

[9] Hattabi, I., et al. "Enhanced Power System Stabilizer Tuning Using Marine Predator Algorithm." *Scientific Reports*, 14, 21548, 2024.

[10] Shahriar, M.S., et al. "Stability Improvement of the PSS-Connected Power System Network with Ensemble Machine Learning Tool." *Energy Reports*, 8, 1163-1173, 2022.

[11] Saadatmand, M., et al. "Robust PID Power System Stabilizer Design Using Interval Analysis." *IEEE Transactions on Power Systems*, 37(4), 3125-3134, 2022.

[12] Khawaja, A.W., et al. "Design of a Damping Controller Using a Metaheuristic Algorithm for Power System Stability." *Applied Sciences*, 12(2), 589, 2022.